

Effect of thermal fluctuations on the average shape of a graphene nanosheet suspended in a shear flow

Gravelle, Simon; Kamal, Catherine; Botto, Lorenzo

DOI

[10.1007/s00707-024-04190-9](https://doi.org/10.1007/s00707-024-04190-9)

Publication date

2025

Document Version

Final published version

Published in

Acta Mechanica

Citation (APA)

Gravelle, S., Kamal, C., & Botto, L. (2025). Effect of thermal fluctuations on the average shape of a graphene nanosheet suspended in a shear flow. *Acta Mechanica*, Article 115207. <https://doi.org/10.1007/s00707-024-04190-9>

Important note

To cite this publication, please use the final published version (if applicable). Please check the document version above.

Copyright

Other than for strictly personal use, it is not permitted to download, forward or distribute the text or part of it, without the consent of the author(s) and/or copyright holder(s), unless the work is under an open content license such as Creative Commons.

Takedown policy

Please contact us and provide details if you believe this document breaches copyrights. We will remove access to the work immediately and investigate your claim.

Green Open Access added to TU Delft Institutional Repository

'You share, we take care!' - Taverne project

<https://www.openaccess.nl/en/you-share-we-take-care>

Otherwise as indicated in the copyright section: the publisher is the copyright holder of this work and the author uses the Dutch legislation to make this work public.



Simon Gravelle · Catherine Kamal · Lorenzo Botto

Effect of thermal fluctuations on the average shape of a graphene nanosheet suspended in a shear flow

Received: 28 June 2024 / Revised: 3 December 2024 / Accepted: 6 December 2024
© The Author(s), under exclusive licence to Springer-Verlag GmbH Austria, part of Springer Nature 2025

Abstract Graphene nanosheets display relatively large hydrodynamic slip lengths in most solvents and, because of this, adopt a stable orientation in a shear flow, instead of rotating, when the effect of thermal fluctuations is not too large (Kamal et al. in Nat Commun 11(1):2425, 2020). In this paper, we combine molecular dynamics simulations and continuum boundary integral simulations to demonstrate that the time-averaged ‘S’ shape adopted by a flexible graphene nanosheet subject to moderate thermal fluctuation is almost identical to the shape predicted for negligible thermal fluctuations. The stable ‘S’ shape adopted by the particle results primarily from the normal hydrodynamic traction, which is sensitive to the orientation of the particle with respect to the flow direction. Our 2D results imply that thermally-induced shape fluctuations may have a relatively minor effect on the time-averaged rheology of dilute suspensions of graphene nanosheets for relatively large but finite Péclet numbers.

1 Introduction

Graphene and other sheet-like nanomaterials have recently attracted the interest of the fluid dynamics community [1,2]. These are nanometrically thin, sheet-like particles which can deform under sufficiently large bending loads. In many applications, such as electronics [3], energy [4], and biomedical technologies [5], these particles are processed in liquids as colloidal dispersions [6–8]. The propensity for deformation under flow of these flexible particles and the rheological behavior of inks made with graphene (or other 2D materials) have therefore become of interest from both the applied and fundamental perspectives [9–14].

In previous studies, we have investigated *rigid* nanosheets of pristine graphene in simple shear flow via molecular dynamics (MD) and continuum boundary integral (BI) simulations [15]. For rigid sheets, we have demonstrated that for slip lengths $\lambda \gtrsim b$, where b is the particle half-thickness, an elongated sheet suspended

Catherine Kamal and Lorenzo Botto have contributed equally to this work.

S. Gravelle (✉)
Univ. Grenoble Alpes, CNRS, LIPhy, 38000 Grenoble, France
E-mail: simon.gravelle@cnrs.fr

C. Kamal
Cambridge Graphene Centre, University of Cambridge, Cambridge CB3 0FA, UK
E-mail: c.kamal@uc.ac.uk

L. Botto
Process and Energy Department, ME Faculty of Mechanical Engineering, TU Delft, Delft 2600 AA,
The Netherlands
E-mail: l.botto@tudelft.nl

Department of Mathematics, University College London, London WC1H 0AY, United Kingdom

in a simple shear flow aligns at a constant small angle with respect to the flow direction [15, 16], rather than rotating as expected for elongated particles without slip [17]. For no-slip particles, a stable alignment has been demonstrated for particles of a particularly complex shape, such as rigid ring-like particles with a non-circular cross-section of the curved solid [18, 19] or boomerang-shaped rigid rods [20]. However, for slip particles, the condition for alignment only requires a plate-like geometry with a small thickness and a slip length greater than the particle thickness [15, 16]. Since graphene is known to display a relatively large hydrodynamic slip length λ in many solvents, [21, 22], much larger than the thickness of the particle $2b$, an alignment of a graphene particle in a shear flow is to be expected. The importance of this observation stems from the fact that non-rotating slip disk-like particles, stably aligned almost parallel to the flow direction, yield a smaller effective viscosity than rotating particles with an average orientation in the flow direction. For dilute suspensions of slip platelets at high Péclet numbers, the effective shear viscosity of the suspension can be even smaller than the suspending fluid viscosity, an anomaly among particulate suspensions [23, 24].

The criterion for alignment, however, depends on the average magnitude of the thermal- or flow-induced fluctuations of the particle's shape [16, 25]. If the magnitude of the particle's shape fluctuation is above a certain threshold, the particle's orientation will change from dynamically stable, where the particle fluctuates about its stable orientation, to unstable, where the particle tumbles. So far, studies to predict the threshold fluctuation for tumbling, for the case of Navier slip particles, have focused on rigid particles [25]. However, for a thin particle in suspension, the assumption of rigidity is only valid for relatively small aspect ratios and applied shear stresses [26]. In the case of single-layer graphene, whose thickness is subnanometric, flexibility and Brownian motion can induce undulations in the shape of the particle, which in turn can affect the particle's orientational distribution. It has been demonstrated using continuum calculations that in the absence of thermal fluctuations, a flexible sheet with hydrodynamic slip assumes a 'S' shape with an orientation angle that is comparable to the one obtained by assuming the sheet to be rigid [26]. However, the effect of flexibility on the attainment of this stable orientation is not completely understood, in particular in the presence of Brownian fluctuations (and possibly other atomistic effects related to the discrete nature of the fluid molecules). An increase in shape deformation may change the stability region of the particle when subject to thermal- or flow-induced shape fluctuations.

In this paper, we combine MD and BI simulations to quantify the average shape of a flexible graphene particle and assess whether Brownian fluctuations in the particle shape are sufficient to induce a reorientation of the particle. The particle is a graphene nanoplatelet having bending rigidity either equal to the one of pristine graphene or having an artificially reduced bending rigidity, where the reduction factor is denoted as α . This modulation of the bending rigidity allows us to investigate deformation effects while still simulating a relatively small particle, a constraint imposed by the high computational cost of MD simulation. The liquid considered is water. The time-averaged shapes extracted from MD for different particle bending rigidities are compared to a model based on the Bernoulli beam equation with hydrodynamic stresses extracted from the BI simulations. Our study extends the knowledge accumulated on the effect of Brownian motion of flexible fibers [27, 28], the most extensively studied type of anisotropic particle, to the case of 2D materials such as graphene. In studies on flexible fibers, the comparison is usually made between continuum simulations and experiments. Here, the comparison is between MD and continuum simulations. We believe that comparison against MD is necessary because the thickness of graphene is comparable to the size of the suspending liquid molecules, so the validity of the continuum assumption needs to be tested.

The MD simulations are carried out for statistically two-dimensional flow in which each sheet has an infinite extent in the vorticity direction. This approach is taken for computational convenience—it allows us to accurately estimate the viscous traction by spatial averaging along the homogeneous direction and keep the computational cost manageable by using domains with limited extent in the spanwise direction—and for amenability to mathematical analysis. We note that previous MD simulations [16] of a fully three-dimensional disk-like nanographene sheet, for values of the Péclet number comparable to those used in the present work, show that the particle's axis of rotation exhibited a random motion in the orientation space of the polar and azimuthal angles (with the polar axis along the vorticity direction). In these simulations, in which the disk exhibited three-dimensional shape deformations, the probability distribution of the polar angle was found to be symmetric, resulting in an average polar angle equal to zero. This result corresponds to a time-averaged planar motion in the flow-gradient plane.

1.1 Simulation details

Molecular Dynamics simulations. MD simulations of a freely suspended graphene particle in a shear flow were performed using LAMMPS [29]. The particle was made of a single graphene layer of approximate length $2a = 3.2$ nm and width $w = 1.7$ nm, with hydrogen atoms terminating the carbon atoms at the edges. The spanwise dimension of the computational domain in the \hat{e}_z direction was equal to the width of the particle, w , and periodic boundary conditions were used in the three dimensions of the space. In this quasi-2D configuration, the particle was free to move within the (\hat{e}_x, \hat{e}_y) plane and to rotate around the \hat{e}_z axis. The fluid was made of a number $N = 2500$ water molecules, enclosed in the \hat{e}_y direction by two moving walls made of iron(II) oxide (FeO) separated by an average distance of 6 nm (Fig. 1a–c). FeO was chosen for its high friction coefficient, which corresponds to a slip length $\lambda \approx 0$ nm in water. A linear shear flow $u_x = \dot{\gamma}y$ with $\dot{\gamma} = 10^{10} \text{ s}^{-1}$ was generated by translating the two walls along the \hat{e}_x direction. The walls were also used to impose the atmospheric pressure $p = 1$ atm to the fluid, thanks to an additional forcing applied in the \hat{e}_y direction. The TIP4P/2005 model was used for water [30]. For the unmodified graphene particle, the all-atom GROMOS force field was used [31]. Particles with reduced bending rigidity were also created by multiplying the dihedral constraints by a factor $1/\alpha$, with $\alpha = 5, 10$, and 100 . The crossed parameters of the Lennard–Jones interaction were calculated using the Lorentz–Berthelot mixing rule. The moving walls and the water were both maintained at a temperature $T = 300$ K thanks to a Berendsen thermostat applied only to the degree of freedom normal to the direction of the flow, and with a time constant of 100 fs. The input and topology files are available in the GitHub repository; see the data availability statement.

Particle orientation from MD. Using the previously described system, production runs of duration 12 ns were performed (for each particle, i.e., for each value of α). During the production runs, the particle configuration was saved every picosecond. For each recorded frame, the instantaneous orientation angles of the tangent to the particle surface at its center and at one of its edges with respect to the laboratory frame (\hat{e}_x, \hat{e}_y) , $\varphi_c(t)$ and $\varphi_e(t)$, were extracted. Then, the instantaneous shape of the particle was analyzed within the particle frame of reference (\hat{e}_s, \hat{e}_n) rotated by $\varphi_c(t)$ relative to the laboratory frame (Fig. 1).

Bending rigidity from MD. The bending rigidity values were measured using loading MD simulations performed in water [32]. The particles were initially maintained flat in the (\hat{e}_x, \hat{e}_z) plane by preventing the motion of the hydrogen atoms at the edge in the \hat{e}_y direction. Then, a constant force of maximum magnitude 3 kcal/mol/\AA was applied along \hat{e}_y to the atoms located at the center of the platelet, to induce a curved shape in the platelet with curvature κ . Both curvature κ and potential energy E_p of the platelet were measured, and the bending rigidity was calculated as $B = 2E_p/(\kappa^2 A)$ [33], where $A = 2(a - b)w$ is the surface area of the platelet, excluded in the edge of size b . Our results for the bending rigidity of pure graphene ($\alpha = 1$) are $B = 1.6 \text{ eV}$, in good agreement with previous simulations [32,34,35] and experiments [36]. For flexible platelets with increasing factor α , our results are $B = 0.43 \text{ eV}$ ($\alpha = 5$), $B = 0.28 \text{ eV}$ ($\alpha = 10$), and $B = 0.14 \text{ eV}$ ($\alpha = 100$). Therefore, the ratio between the bending energy and the thermal energy, $k_B T = 0.0258 \text{ eV}$, where k_B is the Boltzmann constant and $T = 300$ K the temperature, ranges from 0.016 ($\alpha = 1$) to 0.185 ($\alpha = 100$).

Boundary integral simulations. We compare MD simulations to continuum BI simulations of the two-dimensional incompressible Stokes equations. The continuum simulations are non-Brownian and consider an isolated two-dimensional rigid plate-like particle freely suspended in the linear shear flow $u_x = \dot{\gamma}y$. Such simulations have been shown to provide a good estimate of the hydrodynamic stress distribution calculated in MD, provided that (i) a particular reference surface between the carbon and water molecules is used and (ii) a uniform hydrodynamic slip surface is used at the boundary [15,25,37]. For single-layer graphene, a reasonable choice for the reference surface is the surface of a rectangle with rounded ends [15]. The cross-section of the reference surface consists of a rectangular central part of half-length equal to $a - b$ and thickness b and two semi-circular edges of radius b , attached to each end of the rectangle (Fig. 1e). In our simulations, we used a maximum half-length $a = 1.6$ nm and half-thickness $b = 0.25$ nm, in accordance with the particle used in the MD simulations. For the slip surface, a Navier slip boundary condition was assumed with a Navier slip length λ . The slip length was taken as $\lambda = 10$ nm, in agreement with experimental and atomic measurements of hydrodynamic slip of graphene in water [15,21,22,38]. The numerical method for obtaining the hydrodynamic traction is described in detail and verified in Refs. [15,25]. Briefly, the hydrodynamic traction at the particle’s stable orientation is calculated for an undeformed particle as follows. First, the stable orientation angle is determined by evaluating the torque $T(\varphi)$ acting on the particle when it is held fixed with its planar surface parallel ($\varphi = 0$) or perpendicular ($\varphi = \pi/2$) to the flow direction. The torque $T(\varphi)$ is obtained by

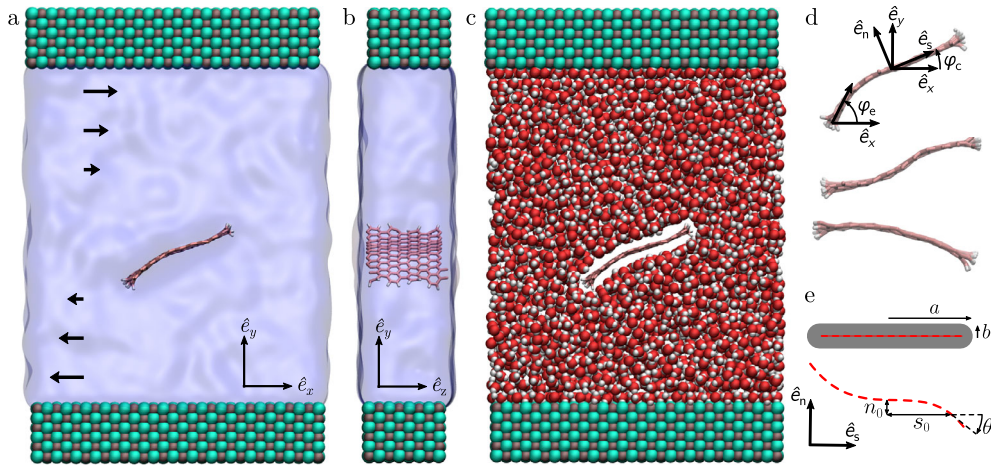


Fig. 1 **a–c** Molecular dynamics system showing the graphene particle immersed in water [39]. The particle has its orientation confined to the flow-gradient plane (\hat{e}_x, \hat{e}_y). The two layers at the top and bottom are the shearing walls, and the undisturbed linear shear flow is $u_x = \dot{\gamma}y$. Water is represented as a transparent continuum field (**a, b**) and as red and white spheres (**c**). The size of the graphene particle along the \hat{e}_z direction, $w = 1.7$ nm, is equal to the size of the computational domain along z (**b**). **d** View of the particle at different times. The top-most snapshot shows the coordinate system with the two angles φ_c and φ_e . The frame of the laboratory is (\hat{e}_x, \hat{e}_y) , and the particle frame of reference is (\hat{e}_s, \hat{e}_n) . The tangent to the platelet at the center of the platelet, \hat{e}_s , is inclined by an angle φ_c with respect to \hat{e}_x . The tangent to the platelet at the edge of the platelet is inclined by an angle φ_e with respect to \hat{e}_x . **e** Schematic of the undeformed (top) and deformed (bottom) flexible particle of half-length a and half-thickness b as modelled in the continuum calculations. The red dashed line is the particle centerline, n_0 and s_0 are the coordinates of the centerline in the particle frame of reference (\hat{e}_s, \hat{e}_n) , and θ is the angle between the tangent of the centerline and \hat{e}_s .

inverting the two-dimensional boundary integral equation numerically to obtain the hydrodynamic traction \mathbf{f} of a two-dimensional particle oriented at the angle φ . The hydrodynamic traction is then used to compute $T(\varphi) = \int_S \mathbf{f} \times \mathbf{x} d\ell$ where S is the boundary of the particle, $d\ell$ is a line element on this boundary, and \mathbf{x} corresponds to a point on S . The stable orientation angle $\langle \varphi_c \rangle$, which for this case is independent of time for $Pe \rightarrow \infty$, corresponds to the value of φ for which $\cos^2(\varphi)T(\varphi = 0) + \sin^2(\varphi)T(\varphi = \pi/2) = 0$ [15]. The hydrodynamic traction is then computed from the boundary integral equation for a particle oriented at $\langle \varphi_c \rangle$. The hydrodynamic traction is used to compute the distributed hydrodynamic load given in the beam equation [see Eq. (5)].

2 Results

The first aspect we address is how the flow affects the orientational statistics of the particle. As shown by the instantaneous snapshots in Fig. 1, the particle attains an average orientation with respect to the laboratory axes, which are fixed with respect to the flow direction. Due to the sheet deformation, each element is characterized by its own rotation angle. To quantify the orientational statistics, we focus on two characteristic angles: the angle φ_c between the tangent unit vector, \hat{e}_s at the mid-point of the sheet and the fixed \hat{e}_x vector, and the angle φ_e between the tangent at one of the edges (the left one in Fig. 1d) and the \hat{e}_x axes. The time series of φ_c and φ_e are shown in Fig. 2a, b. The corresponding probability distribution functions are shown in Fig. 2c, d. Panels a and c in Fig. 2 show data for the pristine graphene sheet, while panels b and d are for the graphene sheet with artificially reduced bending rigidity, $\alpha = 100$.

The time series shows that φ_c and φ_e fluctuate in time around a time-averaged angle $\langle \varphi \rangle = 0.25$. The most probable angle is $\bar{\varphi} = 0.29$. As the bending rigidity decreases, the amplitude of the fluctuations increases, and the correlation between the fluctuations in φ_c and φ_e decreases. The orientational probability distribution functions, which are symmetric about the average, are essentially zero outside the range $[-\pi/6, \pi/3]$. If the sheet performed a tumbling motion, the probability would be nonzero for any value of φ_c , so we infer that our sheets do not tumble. This behavior is confirmed by visual monitoring of the sheets in the MD simulations. Our results also reveal that $p(\varphi_e)$ is slightly broader than $p(\varphi_c)$. This feature is particularly visible for the most flexible particles considered here (Fig. 2c, d).

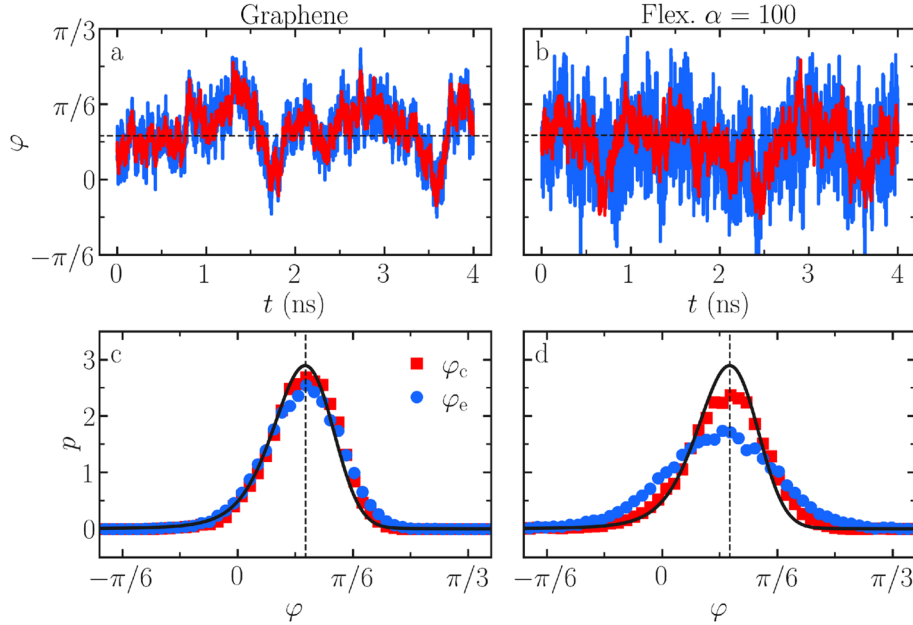


Fig. 2 **a** and **b** Angle at the center, φ_c (red), and at the edge, φ_e (blue), of the particle as a function of time t , for a graphene particle (**a**) and a flexible particle with $\alpha = 100$ (**b**). The dashed horizontal line is the most probable angle $\bar{\varphi} \approx 0.29$. **c**, **d** Orientational distribution function corresponding to the mid-point angle (red squares) or edge angle (blue disks), for a graphene particle (**c**) and a flexible particle with $\alpha = 100$ (**d**). The vertical dashed line is the most probable angle $\varphi \approx 0.29$. The blue and red symbols are results from MD, and the full black line corresponds to the solution of Eqs. (1–3) for a rigid particle with effective aspect ratio $k_e = 0.4i$ (i.e., a particle with large hydrodynamic slip) and rotational diffusion coefficient $D_r = 1.2 \cdot 10^8 \text{ s}^{-1}$ (i.e., $Pe = 90$).

A suppression of tumbling motion is expected from the theory developed for rigid sheets [15,16,40]. According to this theory, at sufficiently high rotational Péclet number, Pe , a rigid sheet is expected to remain aligned at a small constant angle $\langle \varphi \rangle = \varphi^*$ with respect to the flow direction when the hydrodynamic slip length λ is larger than approximately the half-thickness b . For graphene in water, the slip length is relatively large, typically $\lambda \geq 10 \text{ nm}$ [21,22,38], while $b \approx 0.3\text{--}0.4 \text{ nm}$ [15] for single-layer graphene. So, for sufficiently high Pe , our sheets are predicted to maintain a stable orientation, provided that the sheet deformation is sufficiently small for the rigid sheet theory to hold.

For sheets whose shape does not deviate significantly from a straight sheet, a 2D model for the orientational distribution function p at finite Pe can be developed using the theory for rigid sheets. The basic ingredients of such a model are a diffusive flux, $D_r \partial p / \partial \varphi$, which tends to bring φ away from the equilibrium angle φ^* , and a convective flux of magnitude $\Omega(\varphi) \dot{\gamma} p$ which tends to bring φ toward φ^* [16]. The corresponding Fokker–Planck equation reads

$$\frac{\partial p}{\partial t} = \frac{\partial}{\partial \varphi} \left(D_r \frac{\partial p}{\partial \varphi} - \Omega(\varphi) \dot{\gamma} p \right), \quad (1)$$

where $\Omega(\varphi) \dot{\gamma}$ is the hydrodynamic angular velocity, $\dot{\gamma}$ is the shear rate, and D_r the rotational diffusion coefficient of the particle [41]. We seek steady solutions of this equation. For a rigid anisotropic particle, a classical solution due to Bretherton [42,43] provides an exact expression for $\Omega(\varphi)$ as a function of a scalar parameter k_e :

$$\Omega(\varphi) = - (k_e^2 \cos^2 \varphi + \sin^2 \varphi) / (1 + k_e^2). \quad (2)$$

In most studies of anisotropic particles, k_e is regarded as a real number. However, if k_e is real, no steady solution can be found for $Pe \rightarrow \infty$ (as can be seen by setting $D_r = 0$ in Eq. (1) and noting that $\Omega(\varphi) < 0$ for any φ if k_e is real). A steady solution for $Pe \rightarrow \infty$ and fluctuations around the steady solution for finite Pe require k_e to be complex imaginary so that $\Omega(\varphi)$ admits a zero. An imaginary solution can occur if the slip length is sufficiently large, the case considered in the current paper.

The parameter k_e is defined as [44]

$$k_e = \sqrt{\frac{T(\varphi = 0)}{T(\varphi = \pi/2)}}, \quad (3)$$

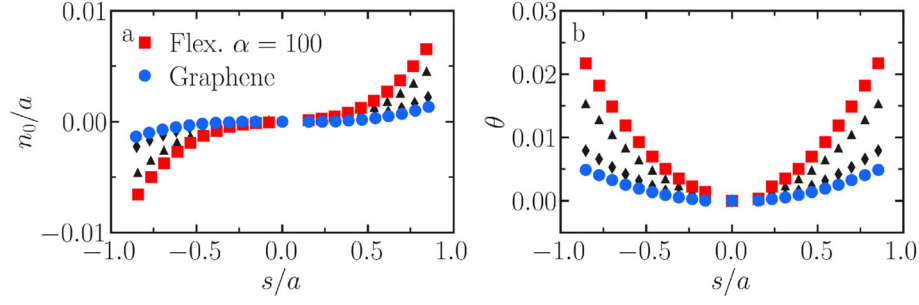


Fig. 3 **a** Time-averaged shape profiles in the particle reference frame (\hat{e}_s, \hat{e}_n). The data corresponds to an unmodified graphene particle (blue disks), and a modified particle with reduced bending rigidity, with $\alpha = 5$ (gray diamonds), $\alpha = 10$ (gray triangles), and $\alpha = 100$ (red squares). **b** Time-averaged rotation angle θ corresponding to the data in panel a.

where $T(\varphi = 0)$ and $T(\varphi = \pi/2)$ are the hydrodynamic torques on a particle held fixed parallel and perpendicular to the flow, respectively. To compare the theory [Eqs. (1–3)] with the MD data, k_e was calculated from the MD simulations by measuring the torque applied by the fluid on a rigid graphene nanosheet oriented at either $\varphi = 0$ or $\pi/2$. With a shear rate $\dot{\gamma} = 10^{10} \text{ s}^{-1}$, time-averaged torques of $-(6.9 \pm 0.9) \text{ kcal/mol}$ and $(36.6 \pm 0.9) \text{ kcal/mol}$ were measured for, respectively, $\varphi = 0$ and $\varphi = \pi/2$, and a value $k_e = (0.4 \pm 0.1)i$ is calculated using Eq. (3).

We solved Equation (1) for $k_e = 0.4i$ and $\text{Pe} = 90$ using the spectral method described in Ref. [25]. An excellent agreement was found between the MD simulations and the theory [Eqs. (1–3)] (Fig. 2c, d). The main difference between the model and the MD results is that the variance of the angular distribution from MD is slightly larger than the variance predicted by Eqs. (1–3), particularly for the most flexible particle considered here ($\alpha = 100$). The value of 90 used for the Péclet number when solving Eqs. (1–3) corresponds to a rotational diffusion coefficient $D_r = \dot{\gamma}/\text{Pe} = 1.1 \cdot 10^8 \text{ s}^{-1}$ with $\dot{\gamma} = 10^{10} \text{ s}^{-1}$. This value is in excellent agreement with the estimate $D_r \approx 3k_B T/32\eta a^3 \approx 1.1 \cdot 10^8 \text{ s}^{-1}$ for an infinitely thin rigid disk of radius $a = 1.6 \text{ nm}$, where k_B is the Boltzmann constant and T is the temperature [45]. Therefore, the comparison between the model prediction and the data is obtained with no free parameters. The only parameter, k_e , was obtained from MD. In principle, k_e could also be calculated from our boundary integral simulations, assuming the particle is rigid [15]. By doing so, we find $k_e = 0.4i$, which agrees with the MD value.

We now examine the time-averaged shape of the sheet, obtained by averaging the positions of the solid atoms from the MD results within the particle frame of reference (\hat{e}_s, \hat{e}_n). The profiles of the averaged longitudinal centerline of the sheet $\mathbf{x}_0 = (s_0, n_0)$ show a characteristic ‘S’ shape (Fig. 3a), with the largest average deformations obtained for the most flexible sheet considered ($\alpha = 100$). We then extract the rotation angle, θ , between the tangent to the centerline and the \hat{e}_s axis (see Fig. 1e). The rotation angle θ , is maximum at the edges, and the more flexible the sheet, the larger the maximum value of θ (Fig. 3b).

The time-averaged shape profile at $\text{Pe} \simeq 90$ displays an S-shape, as does the steady profile at $\text{Pe} = \infty$ [26]. It is therefore natural to attempt to model the time-averaged shape of the sheet using the hydrodynamic load obtained from steady BI simulations at $\text{Pe} \rightarrow \infty$. To do so, we first parameterize the center line by its arc-length $\{s : -a \leq s \leq a\}$. In terms of s , n_0 and s_0 obey the kinematic relations

$$\frac{\partial n_0}{\partial s} = -\sin(\theta), \quad \frac{\partial s_0}{\partial s} = \cos(\theta), \quad \frac{\partial \theta}{\partial s} = \kappa, \quad (4)$$

where κ is the curvature and $\theta = 0$ at the sheet’s midpoint $s = 0$. Treating the flexible object as a slender linear elastic inextensible moving in the flow-gradient plane, the governing equation for θ is [26, 46]

$$\hat{B} \frac{\partial^3 \theta}{\partial s^3} = g_{\perp} + \frac{\partial q}{\partial s}, \quad (5)$$

where $g_{\perp}(s)$ is the average surface traction directed in the normal direction to the center line, and $q(s)$ is the torque density applied by the fluid to the particle, respectively. The parameter

$$\hat{B} = \frac{B}{\dot{\gamma} \eta L^3} \quad (6)$$

is the non-dimensional the bending rigidity for a plate [26], also referred to as the elasto-viscous number [10,47]. Treating graphene as a homogeneous solid, $B \approx B_0 b^3$ [48,49]. In our simulations, we set $B_0 \approx 2.3 \times 10^{11} \text{ N m}^{-2}$, which is inline with reported values the bending rigidity for graphene [50]. Equation (5) is similar to the large-bending deformation model used for a 1D fiber [28] and is equivalent to the Bernoulli beam equation when the deformation is small [26,46]. The difference with equivalent models for fibers is in the computation of the hydrodynamic forcing, $g_\perp + \partial q / \partial s$. In our case, the forcing is computed from the BI simulations, and not from a slender body approximation as usually done in the case of fibers [28].

The difficulty in predicting the shape of the centerline of the sheet lies in the prescription of the loads g_\perp and q , as well as, the edge loads. To distinguish the edge load from the load on the rest of the structure, we split the centerline into two regions: a slender region of length $2L$ for $-L \leq s \leq L$ and ‘edge’ regions for $L < |s| \leq a$ [26,51]. Defining the half-thickness b , then $L = a - b$. The slender region is assumed to satisfy the Bernoulli beam equation, with external force and torques applied from the edge region. Equation (5) is supplemented with the following boundary conditions:

$$\begin{aligned} \hat{B} \left. \frac{\partial^2 \theta}{\partial s^2} \right|_{s=\pm L} &= -q(\pm L) + F_{e,\perp}(\pm L), \\ \hat{B} \left. \frac{\partial \theta}{\partial s} \right|_{s=\pm L} &= T_e(\pm L), \\ \theta|_{s=0} &= 0, \end{aligned} \quad (7)$$

where $F_{e,\perp}(\pm L)$ and $T_e(\pm L)$ correspond to the applied normal force and torque from each edge, respectively.

To solve Eqs.(5–7), values for the distributed and edge loads g_\perp , q , $F_{e,\perp}$ and T_e are needed. We have calculated these values from our BI simulations for a straight (undeformed) geometry, solving for the hydrodynamic traction around the rigid particle oriented at its stable orientation $\tan \varphi = |k_e|$ [15]. The details of these simulations are given in the ‘Simulation Details’ section.

The calculation of g_\perp and q proceeds as follows. The surface was parametrized as

$$\{S = [s_0(s) \pm h(s) \sin \theta(s), n_0(s) \pm h(s) \cos \theta(s)] : -a \leq s \leq a\},$$

where $h(s)$ is the half-thickness of the particles. The surface traction $\mathbf{f}(s, \pm h)$ is averaged over the center line by considering

$$\mathbf{g} = \mathbf{f}(s, h) + \mathbf{f}(s, -h), \quad \Delta \mathbf{g}(s, h) = \mathbf{f}(s, h) - \mathbf{f}(s, -h). \quad (8)$$

Defining the normal and tangent vector to the center line by $\mathbf{n}(s)$ and $\mathbf{t}(s)$, respectively, the normal traction component $g_\perp(s) = \mathbf{g}(s) \cdot \mathbf{n}(s)$, and the torque density is:

$$q(s) = h(s) [\Delta g_\perp(s) \sin \theta(s) - \Delta g_\parallel(s) \cos \theta(s)], \quad (9)$$

where $\Delta g_\perp(s) = \Delta \mathbf{g}(s) \cdot \mathbf{n}(s)$ and $\Delta g_\parallel(s) = \Delta \mathbf{g}(s) \cdot \mathbf{t}(s)$. The edge forces and torques $F_{e,\perp}$ and T_e were calculated by integration of the stress over the edge surfaces $S_E(-L)$ and $S_E(L)$:

$$T_e(\pm L) = \hat{\mathbf{e}}_z \cdot \int_{S_E(\pm L)} (\mathbf{x} - \mathbf{x}_e) \times \mathbf{f} dS, \quad F_{e,\perp}(\pm L) = \int_{S_E(\pm L)} f_\perp dS, \quad (10)$$

where \mathbf{x}_e is the end point of the slender region (i.e., $s = \pm L$).

The computed values of g_\perp , q , and $g_\perp + \partial q / \partial s$ are shown in Fig. 4. The hydrodynamic load is primarily dominated by g_\perp . This function varies roughly linearly with s away from the edges and peaks near the edges. Since slip affects the hydrodynamic traction in the tangential direction but not in the normal direction, the normal load distribution we report in Fig. 4 is qualitatively similar to that for no-slip particles oriented in the flow direction [15]. This explains why a similar distribution of g_\perp with s is observed for no-slip elongated particles oriented with their major axes parallel to the flow direction [15,52,53].

The computed hydrodynamic load is used in Eqs. (5) and (7) to find θ , and the corresponding deformed shape of the sheet is computed from Eq.(4). A finite difference method is used for the discretization. The normal deflection of the sheet is shown as a solid curve in Fig. 5a. The deflection has been rescaled by a factor \hat{B} to show that the average deflections corresponding to sheets of different bending rigidities are identical up to a multiplicative prefactor, and that the shapes given by the continuum and MD simulations are perfectly overlapping. Furthermore, the values of \hat{B} that give collapse onto a single curve are in agreement with direct measurements of the bending rigidity using the loading simulations described in the simulation details (Fig. 5b).

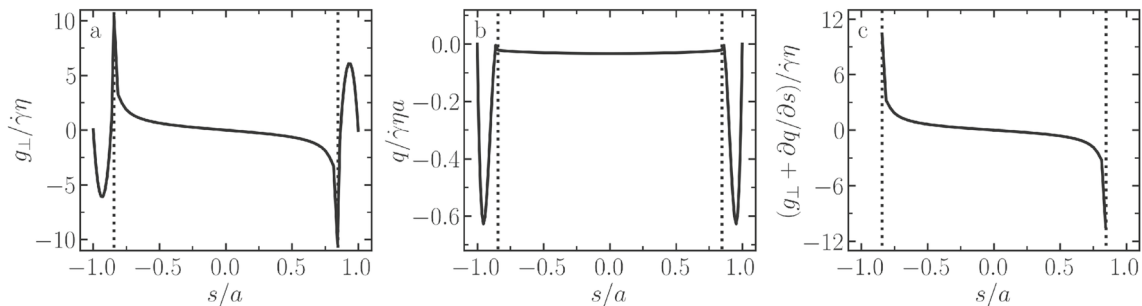


Fig. 4 Hydrodynamic load applied by the fluid on the particle, as computed via BI for a rigid particle, as a function of the coordinate s . Normal component of the traction g_{\perp} normalized by $\dot{\gamma}\eta$ (a), torque density q normalized by $\dot{\gamma}\eta a$ (b), and hydrodynamic load $g_{\perp} + \partial q / \partial s$ normalized by $\dot{\gamma}\eta$ (c). The particle is oriented at $\varphi = 0.3$. The vertical dotted lines represent the boundaries between the slender region and the edge region

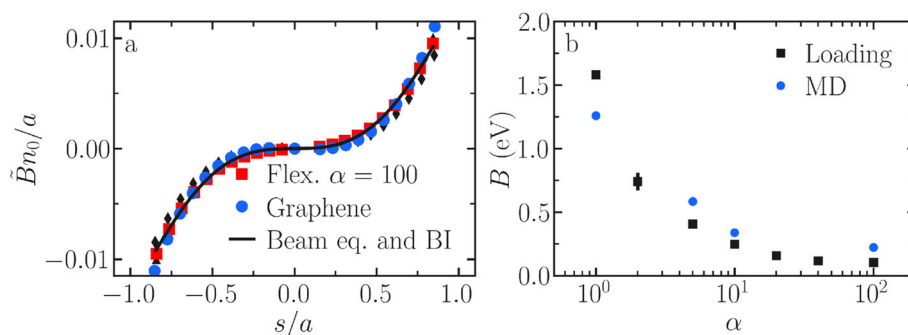


Fig. 5 **a** Comparison of rescaled deflection $\hat{B}n_0/a$ from the continuum calculations (Beam eq. + BI, full line) and from the MD simulations (symbols). The MD data correspond to an unmodified graphene particle (blue disks), and a modified particle with decreased bending rigidity, with $\alpha = 5$ (gray diamonds), $\alpha = 10$ (gray triangles), and $\alpha = 100$ (red squares). The continuum calculations correspond to the solution of the beam equation [Eq. (5)] with the loads (g_{\perp} , q , $F_{c,\perp}$, and T_c) calculated using BI, see the text for details. **b** Bending rigidity B of the particles as a function of the factor α , where $\alpha = 1$ corresponds to pristine graphene, obtained from direct loading measurements (black squares; see ‘Simulation details’) and by matching MD profiles in panel (a) to the continuum model (blue disks).

Because \hat{B} is numerically close to the value obtained from independent MD measurements of the bending rigidity, the agreement between the continuum solution of the beam equations and the MD data for the sheet deflection can be considered to be achieved without resorting to free parameters.

3 Conclusions

We have presented the first direct comparison between Molecular Dynamics and continuum simulations of the time-averaged shape of a flexible graphene nanosheet in shear flow. The graphene sheet has a slip length larger than its thickness and therefore does not perform a full tumbling motion but fluctuates about a preferred orientation angle $\langle \varphi_c \rangle$. In our case we found $\langle \varphi_c \rangle = 0.25$, meaning the particle is nearly aligned with the flow direction. The main result is that the time-average of the fluctuating shape at a finite rotational Péclet number, $Pe \simeq 90$, is, remarkably identical to the steady shape at $Pe = \infty$ (athermal simulations). The sheet’s shape is that of an ‘S’. This ‘S’ shape has also been predicted for no-slip fibers, along with other deformation modes [54]. However, the difference is that here the ‘S’ shape is the time-averaged shape of a fluctuating object that does not perform full rotations, while in the case of fibers it is an instantaneous shape of a rotating object. Shape deformations in our simulation are due to the combination of thermal (Brownian) and flow-induced forces.

The S-shape is accurately predicted by an elastic beam model, where the load is extracted from the hydrodynamic load on a flat plate. This approximation is possible because the deformation is not large, a consequence of the fact that a slip sheet, unlike a no-slip sheet, never reaches the compressional axis of the flow [16,26].

We are also able to calculate the probability distribution function of the orientation of the midpoint of the sheet. The measured time-averaged orientation angle from MD is approximately equal to the instantaneous orientation angle at infinite Péclet numbers for a *flat* slip plate. Importantly, the instantaneous shape fluctuations do not bring the particle outside the region of stable orientation.

The results of this paper are comforting because they suggest that in the study of the orientational and deformation statistics of graphene, one can rely on the statistics of the hydrodynamic load on flat rigid slip plates, at least for sheets that are not too long. The successful application of a theory for rigid particles to flexible particles results from the fact that in our paper the particle is close to its (athermal) equilibrium shape and orientation. For highly deformed particles, like long graphene particles of linear dimension significantly larger than $1\ \mu\text{m}$, or for small Pe , these assumptions may have to be reconsidered, particularly if the deformations induce the particle to rotate and explore the full orientational space. Indeed, the stable hydrodynamic well in which the sheet orientation is trapped depends on the parameter $|k_c|$, which itself depends on the particle aspect ratio [25]. Due to computational limitations, the behavior of long sheet-like particles cannot be explored using all-atom MD. The use of coarse-grained atomic simulation models may help explore this regime in the future [55]. If the particle's orientation becomes unstable, we expect buckling or even chaotic tumbling orbits, similar to those characterizing no-slip sheets [47, 56–58] or fibers [27, 28].

Our calculations were performed for quasi-2D particles with their normals in the flow-gradient plane. An analysis of deformation in full 3D would be interesting, as it could give insights into torsional modes of deformation. The analysis of the trajectories of fully 3D ellipsoids is the subject of ongoing work. The current study quantifies the impact of the fluctuating shape of the particle on the orientation and average shape of the particle, two quantities that rheological models for dilute solutions of anisotropic flexible particles are sensitive to [27, 28].

Acknowledgements S.G. acknowledges funding from the European Union's Horizon 2020 research and innovation programme under the Marie Skłodowska-Curie grant agreement N° 101065060, project NanoSep. C.K. acknowledges funding from the Royal Society Dorothy Hodgkin fellowship, grant number G119482. L.B. gratefully acknowledges funding from the European Research Council (ERC) under the European Union's Horizon 2020 research and innovation program (grant agreement N° 715475, project FlexNanoFlow).

Declarations

Conflict of interest The authors have no relevant financial or non-financial interests to disclose.

Data availability The LAMMPS inputs for the MD simulations are available in the GitHub repository; <https://github.com/simongravelle/publication-data> [59]. The BI data is available upon request.

References

1. Liu, Y., Xu, Z., Gao, W., Cheng, Z., Gao, C.: Graphene and other 2d colloids: liquid crystals and macroscopic fibers. *Adv. Mater.* **29**(14), 1606794 (2017)
2. Hamze, S., Cabaleiro, D., Estellé, P.: Graphene-based nanofluids: a comprehensive review about rheological behavior and dynamic viscosity. *J. Mol. Liq.* **325**, 115207 (2021)
3. Avouris, P., Xia, F.: Graphene applications in electronics and photonics. *MRS Bull.* **37**(12), 1225–1234 (2012)
4. Brownson, D.A., Kampouris, D.K., Banks, C.E.: An overview of graphene in energy production and storage applications. *J. Power Sources* **196**(11), 4873–4885 (2011)
5. Chung, C., Kim, Y.-K., Shin, D., Ryoo, S.-R., Hong, B.H., Min, D.-H.: Biomedical applications of graphene and graphene oxide. *Acc. Chem. Res.* **46**(10), 2211–2224 (2013)
6. Hernandez, Y., Nicolosi, V., Lotya, M., Blighe, F.M., Sun, Z., De, S., McGovern, I.T., Holland, B., Byrne, M., Gun'Ko, Y.K.: High-yield production of graphene by liquid-phase exfoliation of graphite. *Nat. Nanotechnol.* **3**(9), 563–568 (2008)
7. Rao, C., Gopalakrishnan, K., Maitra, U.: Comparative study of potential applications of graphene, MoS₂, and other two-dimensional materials in energy devices, sensors, and related areas. *ACS Appl. Mater. Interfaces* **7**(15), 7809–7832 (2015)
8. Lalwani, G., Henslee, A.M., Farshid, B., Lin, L., Kasper, F.K., Qin, Y.-X., Mikos, A.G., Sitharaman, B.: Two-dimensional nanostructure-reinforced biodegradable polymeric nanocomposites for bone tissue engineering. *Biomacromol* **14**(3), 900–909 (2013)
9. Yu, Y., Graham, M.D.: Wrinkling and multiplicity in the dynamics of deformable sheets in uniaxial extensional flow. *Phys. Rev. Fluids* **7**(2), 023601 (2022)
10. Perrin, H., Li, H., Botto, L.: Hydrodynamic interactions change the buckling threshold of parallel flexible sheets in shear flow. *Phys. Rev. Fluids* **8**(12), 124103 (2023)
11. Salussolia, G., Kamal, C., Stafford, J., Pugno, N., Botto, L.: Simulation of interacting elastic sheets in shear flow: insights into buckling, sliding, and reassembly of graphene nanosheets in sheared liquids. *Phys. Fluids* **34**(5), 053311 (2022)
12. Yu, Y., Graham, M.D.: Coil-stretch-like transition of elastic sheets in extensional flows. *Soft Matter* **17**(3), 543–553 (2021)

13. Giudice, F.D., Cuning, B.V., Ruoff, R.S., Shen, A.Q.: Filling the gap between transient and steady shear rheology of aqueous graphene oxide dispersions. *Rheol. Acta* **57**, 293–306 (2018)
14. Stafford, J., Uzo, N., Farooq, U., Favero, S., Wang, S., Chen, H.-H., L'Hermitte, A., Petit, C., Matar, O.K.: Real-time monitoring and hydrodynamic scaling of shear exfoliated graphene. *2D Mater.* **8**(2), 025029 (2021)
15. Kamal, C., Gravelle, S., Botto, L.: Hydrodynamic slip can align thin nanoplatelets in shear flow. *Nat. Commun.* **11**(1), 2425 (2020)
16. Gravelle, S., Kamal, C., Botto, L.: Violations of Jeffery's theory in the dynamics of nanographene in shear flow. *Phys. Rev. Fluids* **6**(3), 034303 (2021)
17. Jeffery, G.B.: The motion of ellipsoidal particles immersed in a viscous fluid. *Proc. R. Soc. Lond. Ser. A Contain. Papers Math. Phys. Character* **102**(715), 161–179 (1922)
18. Singh, V., Koch, D.L., Stroock, A.D.: Rigid ring-shaped particles that align in simple shear flow. *J. Fluid Mech.* **722**, 121 (2013)
19. Borker, N.S., Stroock, A.D., Koch, D.L.: Robust microstructure of self-aligning particles in a simple shear flow. *Phys. Rev. Fluids* **9**(4), 043301 (2024)
20. Roggeveen, J.V., Stone, H.A.: Motion of asymmetric bodies in two-dimensional shear flow. *J. Fluid Mech.* **939**, 23 (2022)
21. Maali, A., Cohen-Bouhacina, T., Kellay, H.: Measurement of the slip length of water flow on graphite surface. *Appl. Phys. Lett.* **92**(5), 053101 (2008)
22. Tocci, G., Joly, L., Michaelides, A.: Friction of water on graphene and hexagonal boron nitride from ab initio methods: very different slippage despite very similar interface structures. *Nano Lett.* **14**(12), 6872–6877 (2014)
23. The effect of Navier slip on the rheology of a dilute two-dimensional suspension of plate-like particles, author=Kamal, Catherine and Botto, Lorenzo. *J. Fluid Mech.* **972**, 1 (2023)
24. Kamal, C., Botto, L.: Flow and rheology of suspensions of two-dimensional cylindrical or anisotropic particles with Navier slip. *Phys. Rev. Fluids* **9**, 074102 (2024)
25. Kamal, C., Gravelle, S., Botto, L.: Effect of hydrodynamic slip on the rotational dynamics of a thin brownian platelet in shear flow. *J. Fluid Mech.* **919**, A1 (2021)
26. Kamal, C., Gravelle, S., Botto, L.: Alignment of a flexible platelike particle in shear flow: effect of surface slip and edges. *Phys. Rev. Fluids* **6**(8), 084102 (2021)
27. Liu, Y., Chakrabarti, B., Saintillan, D., Lindner, A., Du Roure, O.: Morphological transitions of elastic filaments in shear flow. *Proc. Natl. Acad. Sci.* **115**(38), 9438–9443 (2018)
28. Du Roure, O., Lindner, A., Nazockdast, E.N., Shelley, M.J.: Dynamics of flexible fibers in viscous flows and fluids. *Annu. Rev. Fluid Mech.* **51**(1), 539–572 (2019)
29. Thompson, A.P., Aktulga, H.M., Berger, R., Bolintineanu, D.S., Brown, W.M., Crozier, P.S., in 't Veld, P.J., Kohlmeyer, A., Moore, S.G., Nguyen, T.D.: LAMMPS—a flexible simulation tool for particle-based materials modeling at the atomic, meso, and continuum scales. *Comput. Phys. Commun.* **271**, 108171 (2022)
30. Abascal, J.L., Vega, C.: A general purpose model for the condensed phases of water: TIP4P/2005. *J. Chem. Phys.* **123**(23), 234505 (2005)
31. Schmid, N., Eichenberger, A.P., Choutko, A., Riniker, S., Winger, M., Mark, A.E., Van Gunsteren, W.F.: Definition and testing of the gromos force-field versions 54a7 and 54b7. *Eur. Biophys. J.* **40**, 843–856 (2011)
32. Wang, Q.: Simulations of the bending rigidity of graphene. *Phys. Lett. A* **374**(9), 1180–1183 (2010)
33. Lambin, P.: Elastic properties and stability of physisorbed graphene. *Appl. Sci.* **4**(2), 282–304 (2014)
34. Lu, Q., Arroyo, M., Huang, R.: Elastic bending modulus of monolayer graphene. *J. Phys. D Appl. Phys.* **42**(10), 102002 (2009)
35. Wei, Y., Wang, B., Wu, J., Yang, R., Dunn, M.L.: Bending rigidity and Gaussian bending stiffness of single-layered graphene. *Nano Lett.* **13**(1), 26–30 (2013)
36. Nicklow, R., Wakabayashi, N., Smith, H.: Lattice dynamics of pyrolytic graphite. *Phys. Rev. B* **5**(12), 4951 (1972)
37. Luo, H., Pozrikidis, C.: Effect of surface slip on Stokes flow past a spherical particle in infinite fluid and near a plane wall. *J. Eng. Math.* **62**, 1 (2008)
38. Herrero, C., Tocci, G., Merabia, S., Joly, L.: Fast increase of nanofluidic slip in supercooled water: the key role of dynamics. *Nanoscale* **12**(39), 20396–20403 (2020)
39. Humphrey, W., Dalke, A., Schulten, K.: Vmd: visual molecular dynamics. *J. Mol. Graph.* **14**(1), 33–38 (1996)
40. Gravelle, S., Kamal, C., Botto, L.: Liquid exfoliation of multilayer graphene in sheared solvents: a molecular dynamics investigation. *J. Chem. Phys.* **152**(10), 104701 (2020)
41. Leahy, B.D., Koch, D.L., Cohen, I.: The effect of shear flow on the rotational diffusion of a single axisymmetric particle. *J. Fluid Mech.* **772**, 42–79 (2015)
42. Bretherton, F.P.: The motion of rigid particles in a shear flow at low Reynolds number. *J. Fluid Mech.* **14**(2), 284–304 (1962)
43. Kim, S., Karrila, S.J.: *Microhydrodynamics: Principles and Selected Applications*. Dover Publications, Mineola (2013)
44. Cox, R.: The motion of long slender bodies in a viscous fluid part I. General theory. *J. Fluid Mech.* **44**(4), 791–810 (1970)
45. Sherwood, J.: Resistance coefficients for Stokes flow around a disk with a Navier slip condition. *Phys. Fluids* **24**(9), 093103 (2012)
46. Audoly, B., Pomeau, Y.: *Elasticity and Geometry: From Hair Curls to the Non-linear Response of Shells*. Oxford University Press, Oxford (2010)
47. Silmore, K.S., Strano, M.S., Swan, J.W.: Buckling, crumpling, and tumbling of semiflexible sheets in simple shear flow. *Soft Matter* **17**(18), 4707–4718 (2021)
48. Poot, M., Zant, H.S.: Nanomechanical properties of few-layer graphene membranes. *Appl. Phys. Lett.* **92**(6), 063111 (2008)
49. Landau, L., Lifshitz, E., Pitaevskii, L.: *Theory of Elasticity*, vol. VII. Butterworth, London (1995)
50. Lindahl, N., Midtvedt, D., Svensson, J., Nerushev, O.A., Lindvall, N., Isacson, A., Campbell, E.E.: Determination of the bending rigidity of graphene via electrostatic actuation of buckled membranes. *Nano Lett.* **12**(7), 3526–3531 (2012)
51. Pozrikidis, C.: Shear flow over cylindrical rods attached to a substrate. *J. Fluids Struct.* **26**(3), 393–405 (2010)

52. Singh, V., Koch, D.L., Subramanian, G., Stroock, A.D.: Rotational motion of a thin axisymmetric disk in a low Reynolds number linear flow. *Phys. Fluids* (2014). <https://doi.org/10.1063/1.4868520>
53. Żuk, P.J., Słowicka, A.M., Ekiel-Jezewska, M.L., Stone, H.A.: Universal features of the shape of elastic fibres in shear flow. *J. Fluid Mech.* **914**, 31 (2021)
54. Wiens, J.K., Stockie, J.M.: Simulating flexible fiber suspensions using a scalable immersed boundary algorithm. *Comput. Methods Appl. Mech. Eng.* **290**, 1–18 (2015)
55. Ye, T., Pan, D., Huang, C., Liu, M.: Smoothed particle hydrodynamics (sph) for complex fluid flows: recent developments in methodology and applications. *Phys. Fluids* (2019). <https://doi.org/10.1063/1.5068697>
56. Dutta, S., Graham, M.D.: Dynamics of Miura-patterned foldable sheets in shear flow. *Soft Matter* **13**(14), 2620–2633 (2017)
57. Verhille, G.: Deformability of discs in turbulence. *J. Fluid Mech.* **933**, 3 (2022)
58. Funkenbusch, W.T., Silmore, K.S., Doyle, P.S.: Dynamics of a self-interacting sheet in shear flow. *Soft Matter* **20**(22), 4474–4487 (2024)
59. Gravelle, S.: Simongravelle/publication-data (2024). <https://doi.org/10.5281/zenodo.13341067>

Publisher's Note Springer Nature remains neutral with regard to jurisdictional claims in published maps and institutional affiliations.

Springer Nature or its licensor (e.g. a society or other partner) holds exclusive rights to this article under a publishing agreement with the author(s) or other rightsholder(s); author self-archiving of the accepted manuscript version of this article is solely governed by the terms of such publishing agreement and applicable law.